

Enrichment and Pre-Heating in Intragroup Gas from Galactic Outflows

Romeel Davé, Benjamin D. Oppenheimer, Suresh Sivanandam

Astronomy Department, University of Arizona, Tucson, AZ 85721

31 October 2018

ABSTRACT

We examine metal and entropy content in galaxy groups having $T_X \approx 0.5 - 2$ keV in cosmological hydrodynamic simulations. Our simulations include a well-constrained prescription for galactic outflows following momentum-driven wind scalings, and a sophisticated chemical evolution model. Our simulation with no outflows reproduces observed iron abundances in X-ray emitting gas, but the oxygen abundance is too low; including outflows yields iron and oxygen abundances in good agreement with data. X-ray measures of $[O/Fe]$ primarily reflect metal distribution mechanisms into hot gas, not the ratio of Type Ia to Type II supernovae within the group. Iron abundance increases by $\sim \times 2$ from $z \sim 1 \rightarrow 0$ independent of group size, consistent with that seen in clusters, while $[O/Fe]$ drops by $\sim 30\%$. Core entropy versus temperature is elevated over self-similar predictions regardless of outflows due to radiative cooling removing low-entropy gas, but outflows provide an additional entropy contribution below 1 keV. This results in a noticeable break in the $L_X - T_X$ relation below ~ 1 keV, as observed. Entropy at R_{500} is also in good agreement with data, and is unaffected by outflows. Importantly, outflows serve to reduce the stellar content of groups to observed levels. Specific energy injection from outflows drops with group mass, and exceeds the thermal energy for $\lesssim 0.5$ keV systems. Radial profiles from simulations are in broad agreement with observations, but there remain non-trivial discrepancies that may reflect an excess of late-time star formation in central group galaxies in our simulations. Our model with outflows suggests a connection between physical processes of galaxy formation and both pre-heating and enrichment in intragroup gas, though more definitive conclusions must await a model that simultaneously suppresses cooling flows as observed.

Key words: galaxies: formation, X-rays: galaxies: clusters, galaxies: clusters: general, galaxies: abundances, methods: N-body simulations

1 INTRODUCTION

Galaxy clusters are the largest bound structures in the Universe. This oft-repeated phrase captures both their extremeness as well as their simplicity. Clusters are virialized and nearly spherical, their baryons are mostly in the form of a hot intracluster medium (ICM), and their galaxies are nearly all early-types with old stellar populations. The ICM is close to hydrostatic equilibrium with a temperature near the halo’s virial temperature, and is enriched to around one-third solar independent of cluster mass. The only significant subdivision of clusters comes from examining their central gas properties, where they split into cool core (or cooling flow) and non-cool core clusters. Their smaller counterparts, galaxy groups (usually referring to systems with X-ray temperatures below 2 keV or so), share many of these characteristics. The simplest models regard groups as mini-clusters, i.e. bound spheres of hot gas in hydrostatic equilibrium,

whose properties should be self-similar with clusters (e.g. Kaiser 1986; Navarro, Frenk, & White 1995).

But a closer inspection of group and cluster properties reveals many puzzles and complexities. For instance, gas in hydrostatic equilibrium near the centers of groups should be sufficiently dense to have cooling times significantly shorter than a Hubble time (Fabian, Nulsen, & Canizares 1984), and therefore gas should be cooling rapidly onto the central galaxy. Yet X-ray observations show a distinct lack of gas at temperatures below roughly one-third of the system temperature, and little cold gas or star formation is seen in the center (see Peterson & Fabian 2006, for review). Evidently, some source of energy or entropy is acting to prevent gas cooling in the core. Recently, observations of X-ray bubbles in the ICM apparently blown by AGN-driven jets from the central galaxy offer a possible way to balance cooling (McNamara et al. 2007; Dunn & Fabian 2008). Cos-

mic rays (Guo & Oh 2008; Sijacki et al. 2008), conduction (Kim & Narayan 2003; Jubelgas, Springel, & Dolag 2004), and gravitational heating (Kim & Narayan 2003; Burns et al. 2008; Dekel & Birnboim 2008) may also be viable mechanisms.

Another indication of non-gravitational energy injection into intracluster gas comes from scaling relations between cluster X-ray luminosity (L_X), X-ray luminosity-weighted temperature (T_X), and galaxy velocity dispersion (σ). The self-similar model including only gravitational heating predicts $L_X \propto T_X^2$, which is confirmed by hydrodynamic simulations that do not include gas cooling or processes associated with galaxy formation (Navarro, Frenk, & White 1995; Eke, Navarro, & Frenk 1998). Observations indicate $L_X \propto T_X^3$ for clusters (White, Jones, & Forman 1997), and an even steeper relation in groups (e.g. Xue & Wu 2000). This has led to speculation that some feedback process has added a significant amount of non-gravitational energy into the ICM, which would puff out the gas distribution and lower the X-ray luminosity. Such energy injection was dubbed “pre-heating” by Kaiser (1991). Understanding the amount, epoch, and origin of pre-heating has been the subject of many investigations.

An influential paper by Ponman, Cannon, & Navarro (1999) claimed that systems above 1–2 keV showed rising entropy with temperature, while below that temperature all groups had a similar entropy of ~ 100 keV cm². Here entropy is defined as the X-ray weighted temperature divided by the electron density at one-tenth the virial radius to the two-thirds power. While subsequent observations showed that this claimed entropy floor is instead merely a more-gradual-than-expected decline (e.g. Helsdon & Ponman 2000), the question of what elevates the entropy of gas in smaller systems remains unanswered. Entropy has now become the de facto quantity discussed when quantifying pre-heating.

A third, more oblique indication of non-gravitational energy input into the ICM is the presence of metals. The amount of metals, roughly one-third solar in clusters regardless of size, is large when one considers that in the most massive clusters only a few percent of baryons have formed into stars. It is further remarkable that this enrichment level is similar in clusters of all masses despite significant trends with mass in the amount of stars formed (e.g. Gonzalez, Zaritsky, & Zabludoff 2007; Balogh et al. 2007). Enriching the ICM to these levels represents a non-trivial challenge, because stars in cluster galaxies can themselves only provide a metallicity of about one-sixth solar (Portinari et al. 2004). Accounting for intracluster stars can alleviate this discrepancy (Zaritsky, Gonzalez, & Zabludoff 2004; Sivanandam et al. 2008), but the metals still must be removed from galaxies yet be retained in the hot ICM gas. One possibility is that gas stripped off of infalling galaxies can sufficiently enrich the ICM (van Kampen et al. 2007); if so, the enrichment process would not be energetically important. However, it is clear that the diffuse intergalactic medium (IGM) is enriched at as early as $z \sim 6$ by powerful outflows (Aguirre et al. 2001; Oppenheimer & Davé 2006), so perhaps such outflows could also be responsible for enriching intracluster and intragroup gas. If so, outflows might simultaneously provide some level of pre-heating.

In short there are three current puzzles in understanding the physics of the ICM:

- *Cooling flow problem:* Cooling rates of hundreds to thousands of solar masses per year are expected based on simple cluster models, yet the measured amount of cooling gas is at least an order of magnitude less.
- *Entropy problem:* Entropy levels are progressively more elevated over self-similar predictions towards smaller systems.
- *Metallicity problem:* It is unclear how metals are removed from galaxies in such a way as to enrich intracluster and intragroup gas as observed.

Occam’s razor leads one to attempt to solve these issues with a single physical mechanism. Unfortunately, this is difficult. For instance, the solution to the cooling flow puzzle cannot invoke significant star formation (and hence metal production), because little recent star formation is seen in cluster galaxies. Models of entropy injection from supernovae seem to suggest that it is insufficient to solve the entropy problem (Balogh, Babul, & Patton 1999; Bower et al. 2001; Pipino et al. 2002). These days, it is fashionable to mostly neglect the metallicity problem, ascribing it to a change in stellar yields or perhaps even the initial mass function (IMF), and attempt to solve the cooling flow and entropy problems with a single energy source: heating from active galactic nuclei (AGN). However, this has difficulties as well, because the entropy requirements are large (Babul et al. 2002; McCarthy et al. 2002), though more recently analytic models that use AGN in a self-regulated way have had some success (McCarthy et al. 2008).

In this paper we focus on the entropy and metallicity problems, leaving aside the cooling flow issue for now. Previous theoretical studies of the entropy problem have generally assumed some amount of energy or entropy injection at an early epoch, and then attempted to constrain the amount and epoch of pre-heating by evolving systems (either analytically or numerically) to compare with present-day clusters (e.g. Babul et al. 2002; Kay 2004; Borgani et al. 2005). Few attempts have been made to understand or model in detail possible sources of pre-heating. Observationally, there have been attempts to connect pre-heating and metal enrichment, but with limited success. Renzini (2001) argued that galactic winds must be responsible for ICM enrichment, but they could only add a negligible amount of energy. Ponman, Sanderson, & Finoguenov (2003, hereafter PSF03) found that neither isentropic pre-heating nor cooling models can reproduce the entropy structure of intragroup gas. Hence the physics of pre-heating remains a mystery, and the constraints on its amount and epoch remain only loosely connected to physical process of galaxy formation.

Here we take a different approach. We begin with a model for galactic outflows within hierarchical galaxy formation simulations that is constrained by non-ICM related observations, such as high-redshift IGM enrichment and the galaxy mass-metallicity relation. We then study how such outflows impact the enrichment and entropy level of intragroup gas at $z = 0$. We are limited to investigating galaxy groups and not clusters owing to our numerical capabilities, but this is actually desirable because groups fall in a

particularly interesting regime for pre-heating and enrichment processes. The observed turn-down at ~ 1 keV in the $L_X - T_X$ scaling relations (Xue & Wu 2000) indicates that pre-heating energy input is comparable to the system's gravitational energy at group scales. Groups have a significantly larger stellar fraction, yet their metallicity appears to be comparable to or even lower than clusters, indicating that metal transport processes are crucial. Groups are more generally important because they contain the majority of galaxies in the Universe, and simple dynamical arguments suggest that group environments are the most effective for morphologically transforming galaxies through mergers. Hence there appears to be a lot of action at the group scale. Observations of intragroup gas are rapidly improving, and this provides important constraints on models of pre-heating and enrichment. Investigating such constraints is a central theme of this paper.

We have recently identified a model for galactic outflows that is remarkably successful at reproducing a wide range of observations of cosmic chemical enrichment. In Oppenheimer & Davé (2006, hereafter OD06) we used cosmological simulations that incorporate enriched kinetic feedback to show that a certain class of outflow models are particularly successful at matching detailed properties of IGM enrichment, as traced by CIV absorbers in quasar spectra from $z \sim 6 \rightarrow 2$. In Finlator & Davé (2008) we showed that the exact same model was concurrently and fairly uniquely successful at reproducing the observed mass-metallicity relation in galaxies. In Davé, Finlator & Oppenheimer (2006) we showed that such winds are able to reproduce the luminosity functions of early galaxies, significantly suppressing early star formation as needed to solve the overcooling problem. Bouwens et al. (2007) showed that such a model best reproduces the early cosmic luminosity density evolution. The success of a single outflow model in matching such a wide range of observations, albeit mostly at $z \gtrsim 2$, is compelling, and merits investigation into its impact on intragroup and intracluster gas.

The outflow model we have found to be most successful follows scalings predicted by a momentum-driven wind scenario (Murray, Quatert, & Thompson 2005). In such a model, the wind speed scales with the galaxy's circular velocity, while the mass loading factor, i.e. the amount of mass ejected in an outflow as compared to the star formation rate, scales inversely with it. This yields a constant momentum input per unit star formation. We have found that the generic property making this outflow model successful is that early galaxies drive out an amount of mass comparable to or exceeding that formed into stars, at speeds well above the escape velocity of their host halos. While this might seem surprising, it appears to be required for early IGM enrichment (Aguirre et al. 2001), global star formation suppression (Springel & Hernquist 2003b), and establishing the gas and metal content of high- z galaxies (Erb 2008). Intriguingly, this scaling of wind velocity with galaxy size is also observed in local starburst-driven outflows (Martin 2005; Rupke, Veilleux & Sanders 2005), and at $z \sim 1$ in star-forming galaxies (Weiner et al. 2008), providing a connection between rare present-day outflows and the ubiquitous ones at high- z (e.g. Steidel et al. 2004). One notable issue is that for sufficient mass to be ejected, the energetic requirements are large, comparable to the available supernova

energy (Oppenheimer & Davé 2008). Given expected radiative losses, it may be that another source of energy besides supernovae is required, such as photons from young stars in low-mass galaxies, or AGN in high-mass galaxies. The successes of these momentum-driven wind scalings suggest that we now have a plausible model, albeit phenomenological, of how outflows move mass, metals, and energy on large scales within a hierarchical structure formation scenario.

In this paper we show that cosmological hydrodynamic simulations incorporating momentum-driven outflow scalings are able to simultaneously enrich intragroup media, reduce the stellar fraction to observed levels, and match the entropy levels of observed groups. We compare simulations with and without winds to assess the impact of outflow metal and energy injection. We find that radiative cooling is mainly responsible for breaking the self-similarity between groups and clusters, but that outflows provide an additional entropy boost that becomes important in the poorest groups ($T_X \lesssim 1$ keV). A key aspect of outflows is that they suppress star formation, because cooling-only models can match intragroup medium entropy levels only at the expense of excessive stellar content. Our results suggest that pre-heating and enrichment in groups today arise from the same outflows that are required to distribute metals in the cosmos and regulate early star formation.

In §2 we describe our Gadget-2 simulations with our chemical evolution and outflow modeling. In §3 we study the enrichment properties of intragroup gas in these models, including alpha element ratios and evolution from $z = 1 \rightarrow 0$. In §4 we examine entropy levels and scaling relations in intragroup gas, and quantify energy injection from outflows. In §5 we compare radial profiles of physical properties to data, and study the impact of outflows on such profiles. We summarize in §6.

2 SIMULATIONS

2.1 Simulations with outflows

We run cosmological hydrodynamic simulations using GADGET-2 (Springel 2005), a cosmological Tree-Particle Mesh-Smoothed Particle Hydrodynamics code including radiative cooling and star formation (Springel & Hernquist 2003a). Our version (Oppenheimer & Davé 2008, hereafter OD08) also includes metal-line cooling (Sutherland & Dopita 1993), uses a (spatially-uniform) cosmic photoionizing background given by Haardt & Madau (2001).

We include the effects of galactic outflows and the creation of heavy elements as described in OD08. This builds on our implementation detailed in Oppenheimer & Davé (2006), following Springel & Hernquist (2003a), with three major improvements: (1) We track enrichment contributions from Type II supernovae, Type Ia supernovae, and mass and metal loss from AGB stars; (2) We individually follow carbon, oxygen, silicon, and iron enrichment; (3) We use galaxy baryonic masses (rather than the local gravitational potential) to estimate the galaxy parameters from which outflow properties are derived, using an on-the-fly galaxy finder. The upshot of these improvements is a more accurate tracking of metal evolution in various phases down to $z = 0$, as well as a

more realistic implementation of the dependence of outflow properties with galaxy size. Our chemodynamical model is broadly similar to that used to study ICM enrichment using GADGET-2 by Tornatore et al. (2007), though some details differ. We employ Bruzual & Charlot (2003) models with a Chabrier IMF for computing stellar evolution.

The differences in our new implementation versus the one in OD06 are motivated primarily by a desire to treat the momentum-driven wind model more accurately. In our old model, we used the local gravitational potential as a proxy for galaxy velocity dispersion. At high- z , when the dominant star-forming galaxy is the central object and halos generally only contain a single large galaxy (i.e. the halo occupation distribution lies on the plateau portion; e.g. Berlind et al. 2003), this is a reasonable assumption. At low- z , as halos grow, satellites become more numerous and house more of the total star formation, this becomes a poorer assumption. A galaxy driving an outflow does so locally, and does not necessarily know about the halo in which it resides. Hence in OD08 we moved to identifying individual galaxies and using their properties rather than the global halo properties to derive wind parameters. In OD08 we presented a detailed comparison of the resulting global and IGM enrichment properties between our implementations, and found that at high- z they gave similar results, but at low- z they differed. We believe our new implementation is more accurate particularly at $z = 0$, so we employ it here, and do not compare to our previous (OD06) implementation.

A key aspect for studies of the ICM is iron enrichment from Type Ia supernovae, included in our new simulations. We employ a Type Ia rate following Scannapieco & Bildsten (2005), who parameterize observations by Mannucci et al. (2005) via a prompt component that tracks star formation plus a delayed component that tracks stellar mass. The formulae and metal yields are detailed in OD08. Metals and energy from delayed Type Ia SNe (coming from stars) are added to the nearest three gas particles. As noted in OD08, the vast majority of iron in the universe is produced in Type II supernovae, but for concentrated stellar systems like groups and clusters, Type Ia's provide a large contribution to the gas-phase iron abundance (see also Tornatore et al. 2007).

As in Springel & Hernquist (2003a), each particle that is eligible for star formation has its star formation rate computed based on a Kennicutt (1998) law, and an appropriate level of enrichment is added based on Type II supernova yields (see OD08). The star-forming particle has some probability to be kicked into an outflow or spawn a star particle. The ratio of those probabilities is given by the mass loading factor η , which is an input parameter to the model. If a particle is selected to be in an outflow, it is kicked with a velocity v_w in a direction given by $\pm \mathbf{v} \times \mathbf{a}$ (velocity cross acceleration), resulting in a quasi-bipolar outflow¹. Wind particles propagate purely gravitationally until they are outside the star-forming region (typically few kpc), at which point they can again interact hydrodynamically with surrounding gas. The following formulae are used to relate the galaxy baryonic mass M_b to the mass loading factor and wind speed for

star-forming particles in that galaxy:

$$\sigma = 200 \left(\frac{M_b}{5 \times 10^{12} M_\odot} \frac{\Omega_m}{\Omega_b} h \frac{H(z)}{H_0} \right)^{1/3} \text{ km s}^{-1}, \quad (1)$$

$$v_w = 4.3\sigma \sqrt{f_L - 1}, \quad (2)$$

$$\eta = \frac{150 \text{ km/s}}{\sigma}, \quad (3)$$

where the first equation is taken from Murray, Quatert, & Thompson (2005), originally based on Mo, Mao, & White (1998). The value of f_L is taken from observations of outflows by Rupke, Veilleux & Sanders (2005), who found that they lie between 1.05–2; we choose a random number in that interval for every outflow event. We include a factor to account for increased photon production in lower-metallicity systems. This wind model is identical in form to the “vzw” model of Oppenheimer & Davé (2006); full details are available in OD08.

Ejected wind particles are hydrodynamically decoupled (i.e. the hydro forces are turned off, but not gravity) until they reach a density one-tenth of the critical density for star formation, or for a maximum period of $20h^{-1} \text{ kpc}/v_w$, which is e.g. $\approx 50 \text{ Myr}$ for $v_w = 500 \text{ km/s}$. This is intended to simulate the outflow blowing a hole through the interstellar medium, which cannot be accurately represented given the smoothed nature of SPH. Dalla Vecchia & Schaye (2008) have investigated the effects of turning on or off hydrodynamic decoupling, and found that it gives significantly different results for high-resolution simulations of disk galaxies. However, we have done similar tests at the cosmological resolution used here, and found little difference in the global enrichment properties; this is perhaps not surprising since the spatial resolution here is $5h^{-1} \text{ kpc}$, and the maximum distance an outflow particle can propagate during the decoupled phase is $\approx 20h^{-1} \text{ kpc}$ (and typically it is much less). One advantage of decoupling, as pointed out by Dalla Vecchia & Schaye (2008), is that it results in better resolution convergence. Of course this may not be desirable if the result converges to a physically incorrect answer, but it at least allows a resolution-independent calibration of the outflow model.

We consider two main runs in this paper. They are identical in every way (including random phases in the initial conditions) with the exception that one includes momentum-driven outflows as described above, while the other does not include outflows. Note that in both cases, thermal energy feedback from supernovae is still accounted for in the multi-phase subgrid model of Springel & Hernquist (2003a); however, the explicitly coupled phases means that such feedback cannot drive an outflow. This is the reason why an explicit outflow model is required (Springel & Hernquist 2003b).

Each run has 256^3 dark matter and 256^3 gas particles in a randomly-generated volume of $(64h^{-1} \text{ Mpc})^3$ (comoving), with a concordance cosmology (Komatsu et al. 2008) having $\Omega = 0.25$, $\Lambda = 0.75$, $n = 0.95$, $H_0 = 70 \text{ km s}^{-1} \text{ Mpc}^{-1}$, $\sigma_8 = 0.83$, and $\Omega_b = 0.044$. The value of σ_8 is slightly higher than that favored from WMAP-5, moving more towards values derived from cluster abundances (e.g. Evrard et al. 2008); the difference is not important for the present work. Initial conditions are generated using an Eisenstein & Hu (1999) power spectrum in the linear regime at $z = 129$ by

¹ Movies can be seen at <http://luca.as.arizona.edu/~oppen/IGM/>.

displacing particles off a grid according to the Zel'dovich approximation. Particle masses are $2.72 \times 10^8 M_\odot$ and $1.27 \times 10^9 M_\odot$ for gas and dark matter, respectively, and the gravitational softening length is set to $5h^{-1}\text{kpc}$ comoving.

2.2 Computing group properties

To identify galaxy groups, we find large bound halos using a spherical overdensity (SO) algorithm, as described in Keres et al. (2005). This algorithm finds particles at local potential minima, then expands spherically around those particles until the mean overdensity enclosed corresponds to the virial overdensity for the assumed cosmology (specifically, $178\Omega^{0.45}\rho_{\text{crit}} = 95\rho_{\text{crit}}$; Eke, Navarro, & Frenk 1998). The outskirts of these systems may not properly follow the ellipticity of real systems (which is often ambiguous anyway), but since the outermost properties contribute little to global group properties particularly when weighted by X-ray emission, this difference is not likely to be important.

To identify galaxies, we use Spline Kernel Interpolative Denmax (SKID; Keres et al. 2005). Groups of galaxies are taken to be SO halos that contain ≥ 5 resolved galaxies. Our galaxy mass resolution limit is given by a stellar mass of $M_* > 8.72 \times 10^9 M_\odot$ (i.e. 64 star particle masses), above which galaxy stellar properties have been shown to be converged (Finlator et al. 2006). For comparison, this mass is $\approx 0.2M_{\text{star}}^*$ (Baldry, Glazebrook, & Driver 2008), where M_{star}^* is the characteristic mass in a Schechter function fit to the present-day stellar mass function.

The X-ray luminosity of individual gas particles is computed using the Astrophysical Plasma Emission Code² (APEC) models (Smith et al. 2001), from the particle's mass, SPH-weighted density, temperature, and metallicity. APEC outputs X-ray spectra, from which the luminosity is computed by summing intensities from 0.5–10 keV, uniformly weighted (i.e. no filter profile is assumed). Restricting to 0.5–2 keV makes little difference for our systems. Contributions to line and continuum emission from individually tracked elements (iron, oxygen, silicon, and carbon, along with hydrogen and helium) are computed separately and summed. Other elements are tied to iron assuming solar abundance ratios (Anders & Grevesse 1989), though because line cooling is dominated by iron and oxygen in the intragroup gas temperature and density regime, this choice makes little difference.

The X-ray luminosity L_X of a given group is the summed X-ray luminosities of all particles within the virial radius. The group temperature T_X is computed as the X-ray luminosity-weighted temperature of gas particles, and all quoted metallicities are also X-ray emission-weighted. The emission weighting is done to mimic observations, which obtain temperatures and abundances by fitting APEC or similar models to X-ray spectra, and hence are effectively measuring luminosity-weighted quantities. Radial profiles are computed by performing similar summations in 25 equal thickness spherical shells about the SO halo center.

2.3 Resolution convergence

In this paper we will not directly present any numerical resolution convergence tests. This is unfortunate, and is not our preferred mode of operation. However, several practical issues limit our ability to directly study convergence for the objects of interest, primarily because the groups we examine in this work are already at the extreme of what we can compute in a random-volume simulations. While we have smaller-volume simulations available, they do not produce any systems in the observed group-mass regime, so direct convergence tests on group properties are not possible. To be specific, our $64h^{-1}\text{Mpc}$ run's largest group is 2 keV, which is already fairly small by X-ray group standards; our $32h^{-1}\text{Mpc}$ run's largest is around 0.5 keV, which then does not allow us to check resolution effects for the observationally relevant 0.5 – 2 keV regime. On the flip side, we cannot run even larger volume simulations given our present computational capabilities, because worsening the mass resolution beyond our $64h^{-1}\text{Mpc}$ run is found to significantly compromise early galaxy formation, which is important because these large bound systems form much of their galaxy population early on. Hence, we are stuck in the uncomfortable position of only having a single combination of mass resolution and volume that can examine the properties relevant for observed galaxy groups. For these reasons, the results in this work must be considered preliminary, and our main goal is to present new physical interpretations for group scaling relations as plausible if not definitive.

Nevertheless, we do have some reason to believe that our results are robust. In OD08 we present resolution convergence studies for cosmic mass, energy, and metal distribution, and the simulation resolution used here is reasonably well converged. We have also checked using a $32h^{-1}\text{Mpc}$ simulation with 256^3 dark matter and gas particles that the group properties at temperatures below 0.5 keV are numerically converged. We hope to be able to run constrained simulations to form individual groups and clusters at higher resolution in the future, but for now we do not take that approach because we would like to compare large statistical samples to observations. However, such a constrained-realization study for clusters was done by Tornatore et al. (2007) also using GADGET-2, with mass resolution comparable to what we use here, and through direct tests they determined that their results are not very sensitive to numerical resolution, at least in the central regions of clusters that dominate the X-ray emission. Hence we believe that our results here should be sufficiently robust to numerical effects, so that our conclusions should be generally correct.

3 METAL CONTENT OF INTRAGROUP GAS

Observations of cluster and group enrichment have been bolstered by the increased sensitivity provided by *Chandra* and *XMM*. It is well known that clusters show an iron abundance of one-third to one-half solar (outside the cool core), essentially independent of cluster size (e.g. Renzini 1997; Peterson et al. 2003; de Grandi et al. 2004). Measurements in the poor group regime ($T_X \lesssim 2$ keV), which have recently become available, show a larger scatter with a tendency towards slightly increased metallicity relative to rich clusters, although the

² http://cxc.harvard.edu/atomdb/sources_apec.html

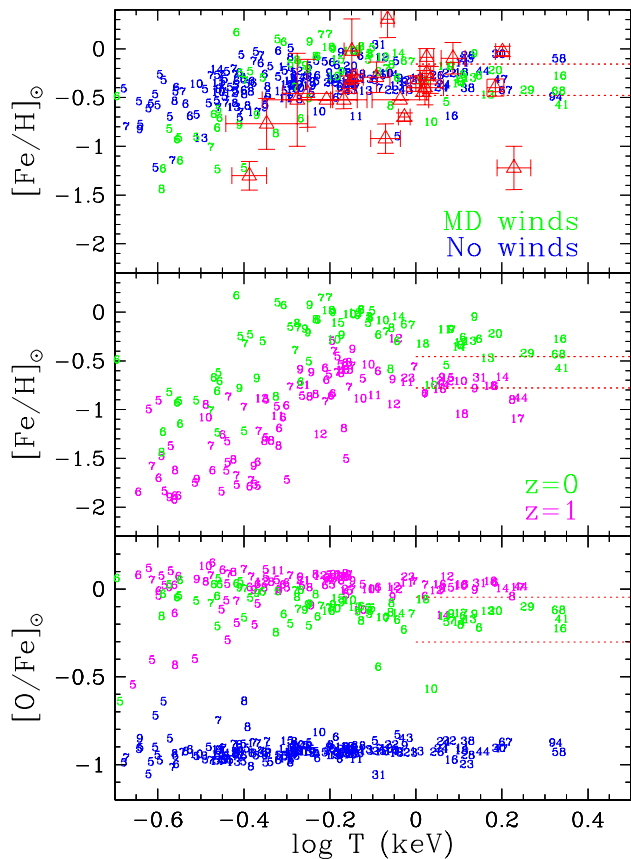


Figure 1. *Top:* $[\text{Fe}/\text{H}]_{\odot}$ (L_X -weighted) for galaxy groups drawn from our momentum-driven simulation (green) and no-wind simulation (blue) at $z = 0$. Small numbers indicate the number of resolved galaxies in the group. Data points (red) from Helsdon & Ponman (2000) are shown for groups. The observed cluster iron abundance range of 0.33 – 0.7 solar (Peterson et al. 2003) is indicated as horizontal dotted lines down to $T_X = 1$ keV. *Middle:* $[\text{Fe}/\text{H}]_{\odot}$ in the momentum-driven wind simulation at $z = 0$ (green, reproduced from above panel) and $z = 1$ (magenta). The observed range at $z = 1$ for comparison is schematically indicated by the dotted lines showing 0.1 – 0.25 solar, i.e. half of the $z = 0$ abundances. *Bottom:* $[\text{O}/\text{Fe}]_{\odot}$ in the momentum-driven (green) and no-wind (blue) simulations at $z = 0$, and the momentum-driven run at $z = 1$ (magenta). Range of $[\text{O}/\text{Fe}]$ observations for clusters at $z \approx 0$ is indicated by the dotted lines (Peterson et al. 2003).

poorest groups seem to reverse the trend and have lower abundances (Davis, Mulchaey & Mushotzky 1999; Helsdon & Ponman 2000). It is puzzling that despite a significant increase in the stellar baryon fraction from the rich clusters to groups (e.g. Gonzalez, Zaritsky, & Zabludoff 2007), no corresponding change is seen in the X-ray gas metallicity. This suggests that the intragroup/intracluster medium metal enrichment is not simply related to the stars formed within the halo potential, and that distribution mechanisms and sources of enrichment play a critical role in governing metallicities. Hence the enrichment level of intragroup gas provides key constraints on such processes (see review by Borgani et al. 2008). In this section we compare our simulations with and without outflows to observations of intragroup gas metallicities.

3.1 Iron abundance

Figure 1 (top panel) shows the iron abundance, weighted by X-ray luminosity, as a function of L_X -weighted temperature T_X for simulated groups. The green points show the results for our momentum-driven wind simulation, and the blue points show the no-wind run. The number of resolved galaxies in each group is indicated by the small number on the plot (in this and subsequent figures). The key result is that the iron abundance hovers around the observed value between one-third and two-thirds solar for $T_x \approx 0.5 - 2$ keV systems. The range of observations for clusters from 1.5–10 keV ($[\text{Fe}/\text{H}]_{\odot} = 0.33 - 0.7$) from Peterson et al. (2003) is shown as the dotted lines. Individual iron abundances for galaxy groups from Helsdon & Ponman (2000) are shown as the red points; observations by Davis, Mulchaey & Mushotzky (1999) show a similar trend. There is a mild trend for lower-mass systems to have higher metallicities down to 0.5 keV, then a significant drop to smaller systems. Qualitatively, this is in agreement with observations, though data on the poorest systems is still highly uncertain.

Matching the observed enrichment level of intragroup gas is a significant success for this outflow model, and indicates that our chemical enrichment model is working together with stellar mass growth to properly enrich X-ray emitting gas. Tornatore et al. (2007) achieved similar success for clusters, with a similarly sophisticated chemical enrichment model implemented in GADGET-2. Hence a metallicity of one-third to one-half solar in intracluster and intragroup gas is achievable using standard yields and initial mass functions, when the cosmic production and distribution of metals is properly incorporated into hierarchical structure formation models. This suggests that non-standard metal yields or initial mass functions (IMFs; Portinari et al. 2004) are not required to match observed abundance levels. In fact, Tornatore et al. (2007) and Fabjan et al. (2008) found that standard yields and a Salpeter IMF provides a better fit to cluster abundances and its evolution than a highly top-heavy IMF.

Perhaps more surprising is that no wind simulation also roughly reproduces the observed iron abundance. One might surmise that this is because the iron content in intragroup gas is dominated by delayed Type Ia supernovae, thereby tracking the stellar mass distribution, and gaseous outflows play a subdominant role. To some extent that is true, but it turns out that the apparent insensitivity of iron enrichment to outflows is something of a coincidence. In reality, the no-wind simulation only matches the iron abundance because it overproduces the amount of stars in groups, thereby compensating for the lack of metal dissemination into intragroup gas. We will return to this point when we examine the baryon fractions in §3.3.

The evolution of the iron abundance has now been measured for massive clusters out to $z \sim 1$. Balestra et al. (2007) and Maughan et al. (2008) found an increase of roughly a factor of two from $z \approx 1 \rightarrow 0$. The middle panel of Figure 1 shows the iron abundance in our momentum-driven case at $z = 0$ (green points) and $z = 1$ (magenta). The dotted lines show the Peterson et al. (2003) range at $z = 0$ lowered by a factor of two, for a rough comparison to the $z = 1$ predictions. Our simulation predicts iron abundance growth that is roughly consistent with that seen in

clusters, though the growth rate seems somewhat higher in the models than in the data. Of course we are comparing simulated groups with observed rich clusters at $z = 1$, so the discrepancy may be due to differential metal evolution between groups than clusters. But the predicted metal increase is independent of system size, at least in the range we can probe with these simulations, so this explanation is disfavored. Another possibility is that our central group galaxies have too much star formation at $z < 1$, since we do not include any feedback mechanism for truncation of star formation. These minor discrepancies aside, the predicted metallicity evolution is generally in agreement with observations.

The outflow simulation predicts a significant drop in metallicity below 0.5 keV or so. This is likely a reflection of the mass-metallicity relation for galaxies setting in (e.g. Finlator & Davé 2008). Poor groups of this size typically house $\sim L_*$ galaxies (such as our Local Group), and below L_* the metallicity of a galaxy begins to drop with stellar mass (Tremonti et al. 2004). Since the mass-metallicity relation is governed by outflows, one would expect the no-wind simulation to show no such drop, and Figure 1 confirms this to be the case. Hence although the star formation efficiency and stellar fractions are higher in smaller groups (as we will see in §3.3), outflows are able to compensate for this by driving more metals out of group potentials. Davis, Mulchaey & Mushotzky (1999) and Helsdon & Ponman (2000) found that the poorest groups in their sample at $T_X \lesssim 1$ keV have lower metallicities (see data points at $T < 1$ keV in Figure 1), but the samples are small and the uncertainties large. Our simulation also predicts an increase in the spread in metallicities at low- T_X , owing to the stochastic nature of outflows; this may help explain the large range of metallicities seen for the poorest groups. As observations improve in this regime, the abundances of the smallest X-ray groups should provide a critical test of outflow models.

3.2 Oxygen abundance

The oxygen to iron ratio is often employed as a diagnostic of the contribution from Type II versus Type Ia supernovae, since oxygen is produced primarily in the former while iron primarily in the latter (at least in groups and clusters). The bottom panel of Figure 1 shows $[\text{O}/\text{Fe}]$ for the momentum-driven wind simulation at $z = 0$ (green points) and $z = 1$ (magenta). These metallicities are X-ray emission weighted, so they trace the enrichment level of hot gas only. Since oxygen enrichment occurs predominantly at earlier epochs coincident with star formation, while Type Ia supernovae enrich in iron over longer cosmic timescales, $[\text{O}/\text{Fe}]$ drops mildly with redshift. Our wind simulations predicts a $\sim 30\%$ drop from $z = 1 \rightarrow 0$, independent of system size. Future observations of ICM alpha element abundances in high- z clusters can test this prediction.

Comparing $[\text{O}/\text{Fe}]$ between our wind (green points) and no-wind (blue) simulations, it is evident that the $[\text{O}/\text{Fe}]$ ratio provides a strong constraint on outflow properties. Without outflows, oxygen is not disseminated effectively into diffuse gas, and instead remain trapped in stars. In our no-wind run, this results in $[\text{O}/\text{Fe}]_{\odot} \approx -1$ at all group masses. Observations of clusters from 1.5 – 10 keV by Peterson et al.

(2003) indicate an oxygen to iron ratio of $70 \pm 20\%$ compared to solar, with no trend versus system size; this range is indicated by the dotted lines in the bottom panel of Figure 1. Our momentum-driven wind run places much more oxygen into X-ray emitting gas, and no trend with system size, in remarkably good agreement with observations. It is notable that a different wind model explored by Tornatore et al. (2007), namely the “constant wind” model of Springel & Hernquist (2003b), was not able to achieve as high $[\text{O}/\text{Fe}]$ ratios as observed. Hence, $[\text{O}/\text{Fe}]$ represents a sensitive test of outflows, which our momentum-driven wind simulation nicely passes.

Contrary to the usual assumption, we find that the $[\text{O}/\text{Fe}]$ ratio in X-ray emitting gas is not a good indicator of the relative numbers of Type II and Type Ia supernovae that have exploded within the group potential. Rather, $[\text{O}/\text{Fe}]$ (and presumably other alpha-to-iron ratios) reflect more the distributions mechanisms of the various elements. This is seen by comparing the bottom panels of Figure 1 and Figure 2. The latter shows the global mass-weighted $[\text{O}/\text{Fe}]$ ratio in our simulated groups, including both stars and cold gas. In both the no-wind and momentum-driven wind simulations, the mass-weighted $[\text{O}/\text{Fe}]$ is around solar, roughly independent of group size. This is in stark contrast to typical values of 0.7 solar in the outflow run, and 0.1 solar in the no-wind case. This arises because oxygen is predominantly distributed into hot gas via winds from galaxies, while iron is predominantly distributed from old stars. When no winds are present, oxygen remains trapped within galaxies, eventually being locked into stars, while iron comes from older stars that can dynamically diffuse out of galaxies directly into hot gas. As a result, X-ray weighted $[\text{O}/\text{Fe}]$ is a sensitive tracer of metal distribution mechanisms, but is not effective as a stellar chronometer.

At face value, our results further imply that tidal and ram pressure stripping of metals out of galaxies falling into deep potential wells is not sufficient to pollute intragroup gas as observed. Such dynamical processes are in principle implicitly included in the no-wind run, yet the no-wind run fails to enrich intragroup gas sufficiently with oxygen. This result apparently contradicts the semi-analytic+N-body simulation results of Kapferer et al. (2007), whose models predict that ram pressure stripping dominates hot gas enrichment for present-day clusters. This may indicate that the simplified modeling used in that work is not capturing the full hydrodynamics. Alternatively, it may be that ram-pressure stripping is numerically suppressed in our simulations. For instance, Agertz et al. (2007) demonstrated that GADGET-2 tends to oversuppress stripping relative to AMR codes, as SPH has trouble modeling hydrodynamical instabilities. Hence while our model of dynamical metal ejection is successful, further testing is required to determine whether gas stripping processes can also be effective.

3.3 Baryon fractions

Figure 2 shows the baryon fractions as a function of halo mass out to r_{500} in our simulations with winds (green points) and without (blue). The top panel shows the fraction of baryons in stars (we do not distinguish stars in galaxies from intracluster/intragroup stars). It is evident that galactic outflows are effective at suppressing star formation on group

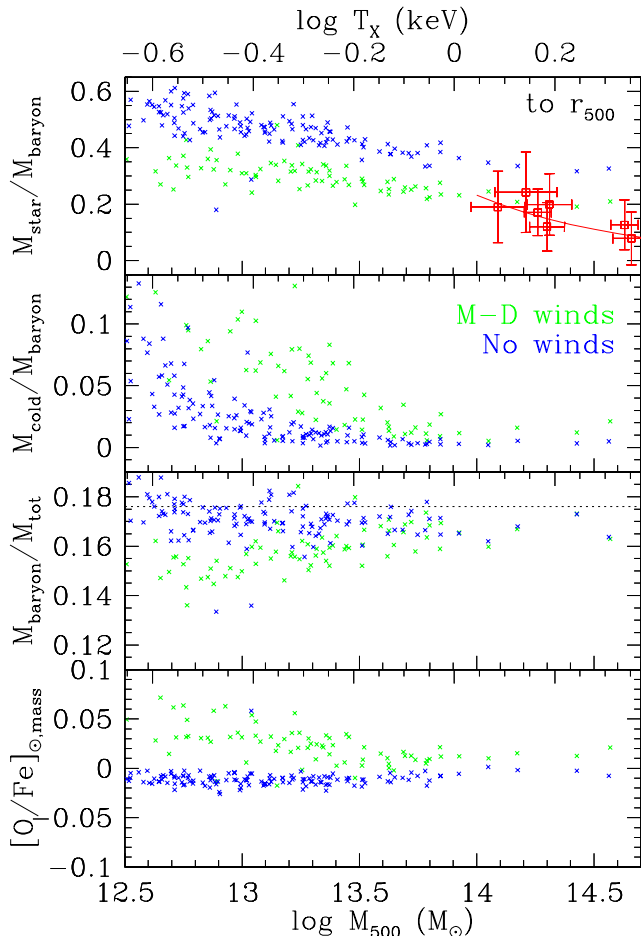


Figure 2. Baryon fractions in various phases, out to r_{500} . Green points are for our favored momentum-driven wind simulation, while blue points are for the no-wind run. *Top:* Stellar baryon fraction, including all stars in the groups regardless of whether they are within galaxies or not. Red points and red line show data and fit to observations of stellar baryon fractions from Gonzalez, Zaritsky, & Zabludoff (2007); their data for groups $< 10^{14} M_{\odot}$ are not shown because they lie beyond the range where the $M_{500} - r_{500}$ relation has been calibrated, so are highly uncertain (A. Gonzalez, priv. comm.). Top axis shows approximate X-ray temperature based on a fit to $M_{500} - T_X$ from our simulations. *Second:* Cold baryon fraction, where cold gas is all gas below 10^6K . *Third:* Baryon fraction with respect to total mass. Dotted line shows the ratio $\Omega_b/\Omega_m = 0.176$ assumed in our simulation. *Bottom:* Log of oxygen to iron mass to iron mass to r_{500} , including both gas and stars, relative to solar ratio. This can be compared to the L_X -weighted $[\text{O}/\text{Fe}]$ in Figure 1.

mass scales. Observational estimates of the stellar fraction on group scales are challenging, primarily owing to the difficulty in constraining the dominant baryonic component in hot gas, but data from Gonzalez, Zaritsky, & Zabludoff (2007), which carefully accounts for intracluster stars, are broadly reproduced in the momentum-driven wind run. As seen in the second panel, there is virtually no cold gas ($T < 10^6 \text{K}$) at least in the range of observed X-ray groups, so baryons not in stars are essentially all in an X-ray emitting plasma. The Gonzalez, Zaritsky, & Zabludoff (2007) stellar fraction data are consistent with data from Lin & Mohr (2004) for $M_{500} > 10^{14} M_{\odot}$ when corrected for ICL light

contributions (Baldry, Glazebrook, & Driver 2008). Below this mass, systematic uncertainties become large.

The most massive groups still have 20% of their baryons in stars, which is too high compared to data, and a simple extrapolation of the simulated group trends to higher masses would clearly violate observations of stellar fractions in rich clusters (typically $\ll 10\%$). Another way to say this is that the observed $f_* - M_{500}$ relation (where f_* is the stellar fraction) is steeper than our simulations predict. Specifically, our simulations yield $d \log f_*/d \log M_{500} = 0.18$ around $10^{14} M_{\odot}$, which is shallower than both Gonzalez, Zaritsky, & Zabludoff (2007) and Lin & Mohr (2004) data, though somewhat steeper than the semi-analytic model predictions of Bower et al. (2006) (as calculated by Baldry, Glazebrook, & Driver 2008). However, this does not necessarily indicate a significant constraint on cold dark matter models (as argued by Baldry, Glazebrook, & Driver 2008). Rather, it probably owes to a lack of suppression of star formation in massive systems in simulations, from AGN feedback or whatever the heating source is that prevents cooling flows.

The suppression of star formation on group scales is not as great as the global suppression: The simulation without winds at $z = 0$ contains 17% of its total baryons in stars, while the wind run has 7%. The latter value is in good agreement with observational estimates (Bell et al. 2003; Baldry, Glazebrook, & Driver 2008). Hence outflows are able to suppress star formation both globally and on group scales in general agreement with observations.

The third panel of Figure 2 shows the mass fraction of total baryons against halo mass. In general, the total baryon fraction is slightly smaller than the cosmic baryon fraction (indicated as the dotted line), owing to increased pressure support that puffs out the hot gas; this is qualitatively consistent with observations (e.g. Gonzalez, Zaritsky, & Zabludoff 2007). Outflows are further able to remove a small but noticeable amount of baryons from halos with masses $\lesssim 10^{14} M_{\odot}$.

Returning to the iron abundance with and without outflows, it is now clear that although simulations without outflows reproduce the observed intragroup metallicities, they do so by forming too many stellar baryons. Outflows therefore serve the dual purpose of suppressing star formation, while transferring sufficient metals from galaxies into the hot gas phase. Furthermore, outflows significantly increase the alpha element ratio in intragroup gas to be in better agreement with observations. Hence our simulations suggest that outflows are likely to be necessary in order to enrich intragroup gas to observed levels.

4 PRE-HEATING

We now turn to studying another aspect of outflows, namely the energy they add to intragroup gas. Entropy levels in intragroup gas are known to be elevated relative to self-similar extrapolations from clusters, but the physical process responsible for pre-heating is unclear. Voit & Bryan (2001) argued analytically that supernova heating together with radiative cooling could yield the observed entropy distribution in groups. Incorporating such feedback processes into simulations has only recently been attempted; for in-

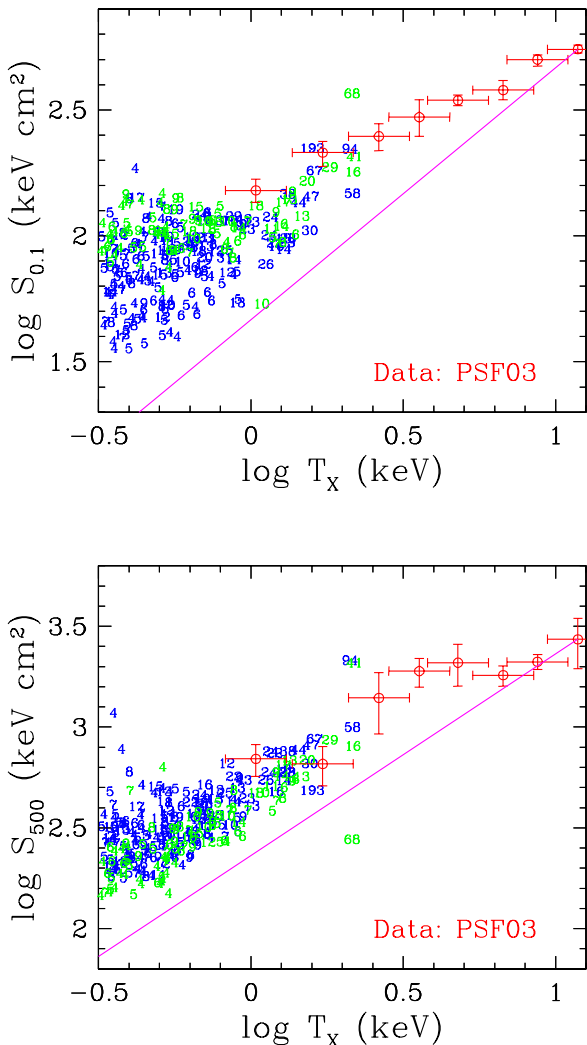


Figure 3. Entropy, defined as $T_X/n_e^{2/3}$, as a function of X-ray temperature for galaxy groups in our simulation with outflows (green) and without (blue). Binned data from PSF03 is shown in red. Expected self-similar scaling, normalized to the most massive data points, is shown as the magenta line. *Top:* Entropy at 10% of the virial radius. *Bottom:* Entropy at r_{500} , roughly two-thirds the virial radius.

stance, Borgani et al. (2005) examined and dismissed a simple model of galactic outflows as the dominant source of pre-heating. Muanwong, Kay, & Thomas (2006) showed that an ad hoc model of energy input proportional to star formation is able to reproduce observed entropy levels, but preliminary comparisons to entropy evolution favored an early pre-heating scenario. None of these works employed an outflow model that is constrained to match external observations. Here we examine whether our momentum-driven wind model, in addition to enriching intragroup gas, is concurrently able to add significantly to its entropy budget.

4.1 Entropy

Figure 3 (top panel) shows entropy $S_{0.1}$ at $0.1R_{\text{vir}}$ as a function of group X-ray temperature, for our momentum-driven wind (green) and no-wind (blue) runs. Entropy

is defined here as $T_X/n_e^{2/3}$, where T_X is the system X-ray luminosity-weighted temperature and n_e is the electron density at a given radius. Data points (binned) from PSF03 are shown, and the expected self-similar scaling normalized to the most massive clusters is indicated by the magenta line. In self-similar scaling, $n_e(0.1R_{\text{vir}})$ is independent of size since groups are scaled-down versions of clusters, hence $S \propto T_X$. As is well-known, $S_{0.1}$ is elevated at group scales relative to a self-similar extrapolation from massive systems. While an entropy floor at $\sim 100 \text{ keV cm}^2$ (Ponman, Cannon, & Navarro 1999) is not seen in the models, more recent observations indicate no floor but merely a more gradual decline than expected. PSF03 finds a best fit of approximately $S_{0.1} \propto T_X^{2/3}$.

Elevated entropies are obtained in both wind and no-wind runs, since radiative cooling is effective at preferentially removing low-entropy intragroup gas over a Hubble time (e.g. Bryan 2000; Voit & Bryan 2001). The low-entropy gas then ends up forming stars. While the entropy trend produced by radiative cooling qualitatively agrees with data, as shown in Davé, Katz, & Weinberg (2002), there are two major difficulties with the radiative cooling solution alone. The first is that the amount of stars produced by the low-entropy gas exceeds observations, as shown in Figure 2 and found previously (e.g. Muanwong et al. 2002). The second is that, as seen in Figure 3, the entropy increase from radiative cooling alone is not quite sufficient to match observations. Hence an alternate source of entropy is still required, preferably one that simultaneously reduces the amount of star formation in groups.

Our momentum-driven outflow model appears to alleviate both problems. We have seen that it reduces the stellar baryon fraction to be in better agreement with observations on group scales. Figure 3 also shows that it raises the entropy level over the no-wind case, particularly for systems with $T_X \lesssim 1 \text{ keV}$, to be in slightly better agreement with the low- T_X end of available observations. An extrapolation of the observed trend ($S \propto T_X^{2/3}$) to lower T_X is also well-matched to the outflow run predictions, which can be fit by $S_{0.1} \propto T_X^{0.6}$ over the temperature range probed. Hence outflows together with radiative cooling appear to provide a viable solution to the entropy crisis in galaxy groups.

The fact that outflows *increase* core entropy is not trivial, since they also suppress cooling, and hence suppress the removal of low-entropy gas. The entropy addition from outflows therefore appears to be (more than) compensating for the reduced stellar fraction. That said, our most massive systems show twice the stellar fraction as observed (see Figure 2), and so some additional mechanism such as AGN feedback is likely required to further suppress star formation at $T_X \gtrsim 1 \text{ keV}$. It is not clear whether such a mechanism would continue to compensate for further reductions in stellar fractions in the way that outflows do. Looking carefully at Figure 3, it does appear that the core entropy is still slightly low for $T_X \gtrsim 1 \text{ keV}$ systems, though it is within uncertainties. Hence it could be that radiative cooling, outflows, and some other feedback mechanism all work together to establish the entropy level in larger groups and clusters. A fully self-consistent model incorporating all these processes is required to assess this.

The entropy in group outskirts is also seen to be elevated with respect to a self-similar extrapolation from clus-

ters. The bottom panel of Figure 3 shows the entropy at r_{500} , roughly two-thirds the virial radius. Observations (PSF03, shown as the red points) are more uncertain here, particularly for groups, but our simulations generally fall in the observed range. S_{500} is mostly insensitive to outflows; it is apparently established by radiative cooling. If anything, the wind run shows marginally lower entropies, probably owing to reduced removal of low-entropy baryons. The $S_{500} - T_X$ relation shows a slope just below unity, unlike $S_{0.1}$ and more in line with expectations from self-similarity. If this would continue to the largest clusters, it would exceed the observed S_{500} ; this will require constrained realization simulations of large clusters to test.

4.2 Outflow energy deposition

We now quantify pre-heating due to outflow energy injection in simulations. During our runs we record the mass and velocity (and hence energy) of particles kicked into an outflow. Ideally, one would like to track where and when this energy gets deposited into surrounding gas; unfortunately, this is not straightforward. So instead, we make a crude estimate of energy input into intragroup gas by assuming that all the outflow particles lying within a group’s hot gas by $z = 0$ have deposited their entire outflow energy into that gas. Note that this estimate may either be an underestimate of the actual energy added if outflow particles lose energy to intragroup gas but end up outside the group, or it may be an overestimate if groups accrete outflow particles that already have deposited most of their energy outside the group’s halo. While this estimate is not exact, it is still instructive.

Figure 4 shows the wind energy per hot baryon deposited as a function of T_X (top panel), and the median age when the energy was deposited (bottom panel), as the green points. The energy is the total outflow energy of all wind particles residing within the hot intragroup gas, divided by the number of baryons in that gas (note that this is not all the baryons in the group). The age is estimated by taking the median of the ejection times of all wind particles within intragroup gas; again, this must be considered a relatively crude estimate of the energy injection time.

The energy deposition per baryon shows a mild decreasing trend with system size. This is at first glance surprising, since in the momentum-driven outflow model the wind energy output per unit star formation scales as $\eta v_w^2 \propto v_{\text{circ}}$ (equation 3). Hence one expects larger systems to have larger energy input. But the baryonic budget serves to counter this trend: Larger groups have a lower stellar fraction and more hot gas over which to spread the energy (Figure 2). The net result is that hot baryons in larger systems are heated slightly less by winds.

The total energy injection into groups from outflows is comparable to the total supernova energy from stars formed in the group (magenta points in Figure 4). The SN energy is computed by taking the total stellar mass in each group and multiplying by 4×10^{48} ergs/ M_\odot for a standard IMF (OD08). As argued in OD08, such high levels of energy input appear to be necessary to provide the cosmic distribution of metals from galactic outflows, and owing to expected radiative losses this level of energy may not be obtainable from supernovae alone (barring IMF variations; e.g. Davé 2008). While we cannot claim to fully understand or model the

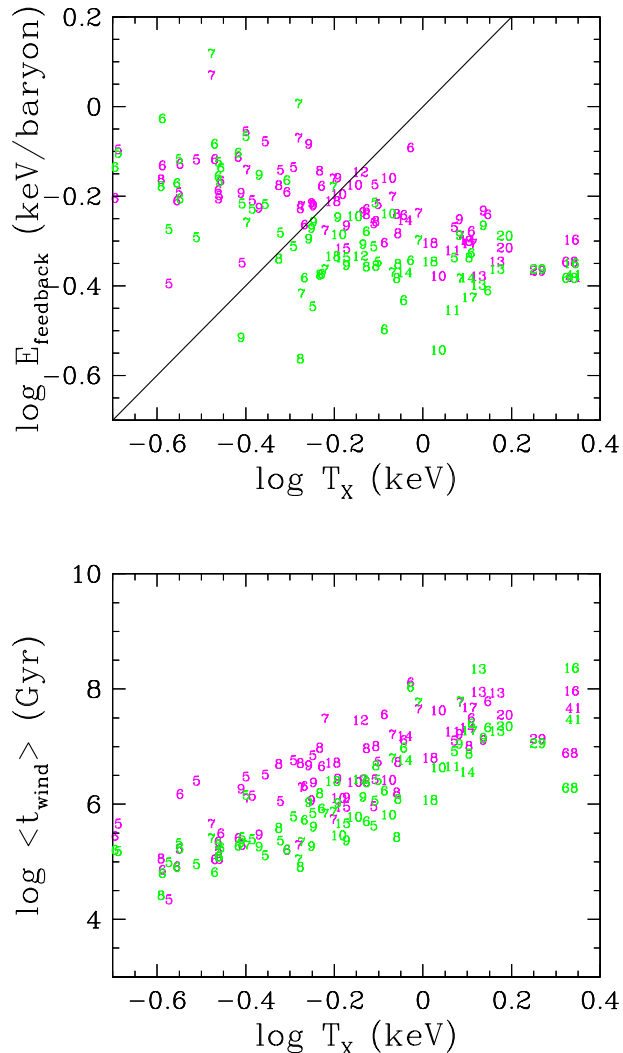


Figure 4. *Top:* Estimated energy per baryon deposited into intragroup gas from galactic outflows (green points), as a function of system temperature. Solid line is the line of equality between wind energy and system thermal energy. Magenta points show supernova energy per hot baryon from all the stars formed within the groups. *Bottom:* Age by which half the energy was deposited (green points), taken to be the median ejection time of all wind particles in the hot intragroup gas. Magenta points show median age of stars in group.

outflow driving mechanism, we note that such energetic outflows seem to be required to match a wide range of observations, not just intragroup gas entropy.

The median energy injection time (green points in bottom panel of Figure 4) is typically fairly recent, with the smallest systems having a median pre-heating age of 5 Gyr ($z \approx 0.5$), while our largest systems at around 2 keV have a typical pre-heating age of 8 Gyr ($z \approx 1$). This can be compared to the median age of star particles in the group (magenta points), which are comparable although slightly older, particularly in the smaller systems. In general it appears that stars in group galaxies are responsible for enriching and pre-heating intragroup gas, as expected. In the future we plan to examine the redshift evolution of hot gas

to determine more precisely where and when outflow energy and metals are deposited.

4.3 Scaling relations

Figure 4 shows that the energy deposition from winds typically exceeds the system’s thermal energy for systems below about 0.5 keV (note the solid line showing equality between T_X and wind energy input). Hence outflows should produce a lowered luminosity for systems near this temperature and below. Here we investigate whether this provides an explanation for the apparent break in luminosity scaling relations near ~ 1 keV, below which the $L_X - T_X$ relation is observed to be significantly steeper (e.g. Xue & Wu 2000).

Figure 5 shows the $L_X - T_X$ (top) and $\sigma - T_X$ (bottom) relations for our simulated groups from our momentum-driven wind run. The $L_X - T_X$ relation shows a clear break around 1 keV, with the power-law slope above and below this break being 2.6 ± 0.6 and 4.9 ± 0.2 , respectively. These slopes agree well with observations: The red dashed line shows a fit to observations of groups and clusters from Xue & Wu (2000); a fit to $L_X - T_X$ for clusters by White, Jones, & Forman (1997, not shown) is quite similar. Green points show data from a ROSAT compilation by Osmond & Ponman (2004); we show all their groups that have measured T_X values, including systems with a small radial extent in observable X-rays (i.e. their “H-sample”) that they exclude from their fits, since we make no such cuts in our simulations. The L_X values used are extrapolated to r_{500} , whereas our simulations include all luminosity out to the virial radius, but this should not be a large difference.

The Osmond & Ponman (2004) $L_X - T_X$ data as well as the Xue & Wu (2000) fit at $T_X < 1$ keV lie systematically below that for the simulated groups. If real, this suggests that there may still be some missing energetic input into low-mass systems.

The no-wind simulation (not shown) also displays a break in the $L_X - T_X$ relation, but it is not as prominent and occurs at a lower T_X . Our no-wind case is in general agreement with simulations (also without outflows) by Davé, Katz, & Weinberg (2002), who argued that cooling alone can produce a break in scaling relations, but this break occurs at ~ 0.3 keV. Hence outflows serve to add enough entropy to move the L_X break closer to the observed location.

The $\sigma - T_X$ relation (bottom panel of Figure 5) shows no break. Here, σ is calculated from the dark matter particles in each simulated group; in Davé, Katz, & Weinberg (2002) it was shown that calculating σ from galaxies yields a similar values so long as there are a sufficient number of galaxies in a group. The simulated groups are best fit by a power-law slope of 0.60 ± 0.02 (solid line), and the fit is remarkably similar to that based on compiled observations of groups and clusters by Xue & Wu (2000, red dashed line). This is slightly different from the self-similar scaling slope of 0.5, and shows that groups at a given mass have elevated temperatures. The no-wind simulation (not shown) shows a similar slope (see Davé, Katz, & Weinberg 2002), indicating that the elevated temperatures occur primarily because radiative cooling has preferentially removed the low-temperature gas.

The scatter in the observational points is considerably larger than in the simulated case. As an example, green points (with errors) on the $L_X - T_X$ plot show individual

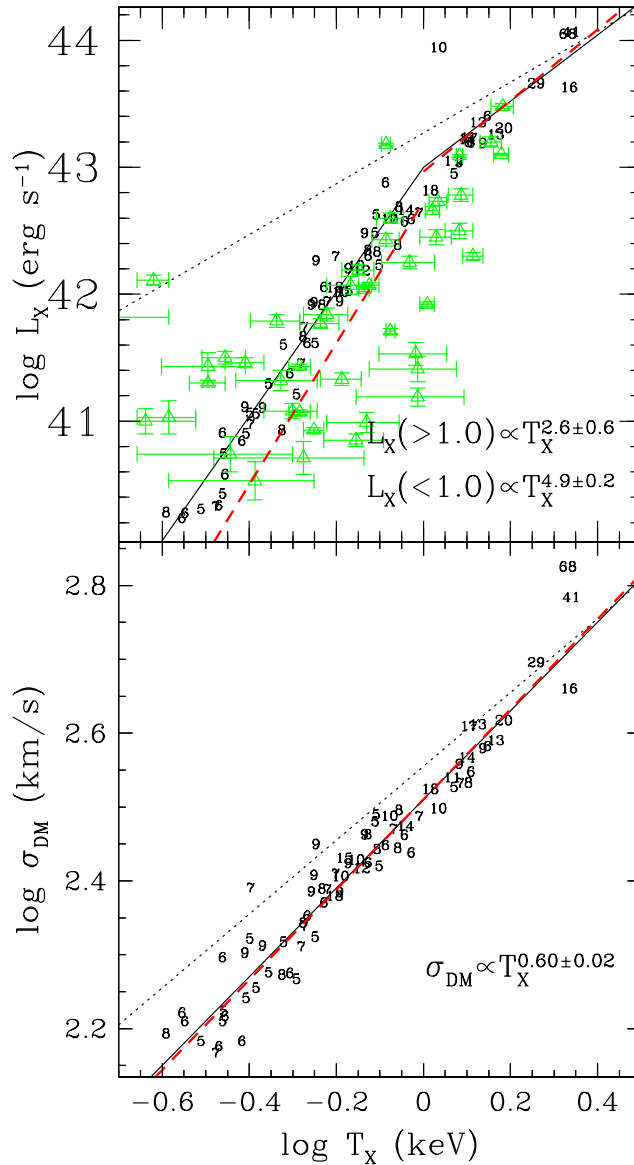


Figure 5. $L_X - T_X$ (top panel) and $\sigma - T_X$ (bottom) relations for simulated groups. Power-law fits are indicated in the lower right, and the fits are shown as the solid lines. Dotted lines show self-similar scaling normalized to the largest systems. Fits to observations of groups and clusters compiled by Xue & Wu (2000) are shown as the red dashed lines. Green triangles show individual group observations from Osmond & Ponman (2004).

measurements from Osmond & Ponman (2004). The large scatter may be due partly to observational systematic uncertainties, but this seems unlikely to provide the bulk of the explanation, since clusters show similar scatter that can be directly linked to their well-measured density and temperature profiles (e.g. Markevitch et al. 1998). It has been suggested that it may instead reflect intrinsic scatter in the level of pre-heating (Balogh et al. 2006). Since our simulations implicitly produce variations in halo concentration and formation epoch, as well as in wind energy deposition, these alone cannot provide the observed scatter (as also argued by Balogh et al. 2006). We leave for the future a careful consideration of observational causes of scatter via making

mock X-ray images and analyzing them alongside real X-ray data. This will also be useful for evaluating the more general bias that observed groups tend to be X-ray bright, but these may not be representative of groups as a whole. The final solution, however, may require some intermittent additional source of heating such as AGN feedback.

In summary, outflows add an important contribution to the entropy budget of poor groups, whose energy input becomes comparable to the system thermal energy at $T_X \sim 1$ keV. Radiative cooling is primarily responsible for breaking self-similarity above this scale, while outflows exaggerate deviations from self-similarity below this scale.

5 PROFILES

With increasingly sensitive observations from *Chandra* and *XMM*, it is now possible to construct radial profiles of group properties. Such profiles provide an added challenge to models, one that simulations have traditionally had a difficult time matching, since they contain more detailed information about metal and energy injection processes. In this section we examine projected radial profiles for physical quantities from our momentum-driven wind simulation.

Figure 6 shows the luminosity, temperature, electron density, entropy, iron abundance, and oxygen to iron ratio profiles as a function of radius, from $\approx 0.06 - 1R_{\text{vir}}$. The inner limit corresponds to $\approx 0.1R_{500}$, which is typically few tens of kpc, and approaches the effective resolution limit of our simulations. As seen in the top panel, the luminosity profile shows a flat central core (similar to observed non-cool core systems; see Davé, Katz, & Weinberg 2002), so the poorly resolved central region does not make a significant contribution to groups' X-ray emission-weighted properties.

We subdivide the groups into two equal-number bins exceeding 0.5 keV, which results in about 40 groups each from 0.5 – 0.7 keV and 0.7 – 2 keV. We then compute the median value among the 40 groups for each physical quantity within each of the 20 radial bins. This yields the median profiles shown within these two temperature ranges. We show such profiles for our momentum-driven wind run (green and magenta) and no-wind run (blue and cyan).

The simulated temperature profiles show a drop by a factor of ~ 2.5 from $0.1 \rightarrow 1R_{\text{vir}}$. The no-wind profiles are well-described by the fit proposed by Loken et al. (2002), namely $T_X \propto (1 + 0.75r/r_{500})^{-1.6}$. With outflows, the profiles are altered slightly in the inner parts, such that they show a flattening and perhaps even a turnover within $\sim 0.2R_{\text{vir}}$. Qualitatively, this is in better agreement with X-ray group profiles from Rasmussen & Ponman (2007), who find a turnover in the temperature profile at $\sim 0.1R_{500}$.

Fits to observed temperature profiles ($\langle T \rangle$) are shown as the red and blue dotted lines in Figure 6, arbitrarily scaled to lie in the range of our simulated groups. Rasmussen & Ponman (2007, red dashed line) measured profiles for 0.3 – 2.1 keV groups, so this is most directly comparable to our simulated systems. We show the Loken et al. (2002) form of the fit to their data, specifically $T_X \propto (1 + 0.75r/r_{500})^{-1.45}$, which is somewhat shallower than the simulated profiles. We also show a fit to cluster profiles by Leccardi & Molendi (2008, blue dashed line). Their analysis is notable because of the careful ac-

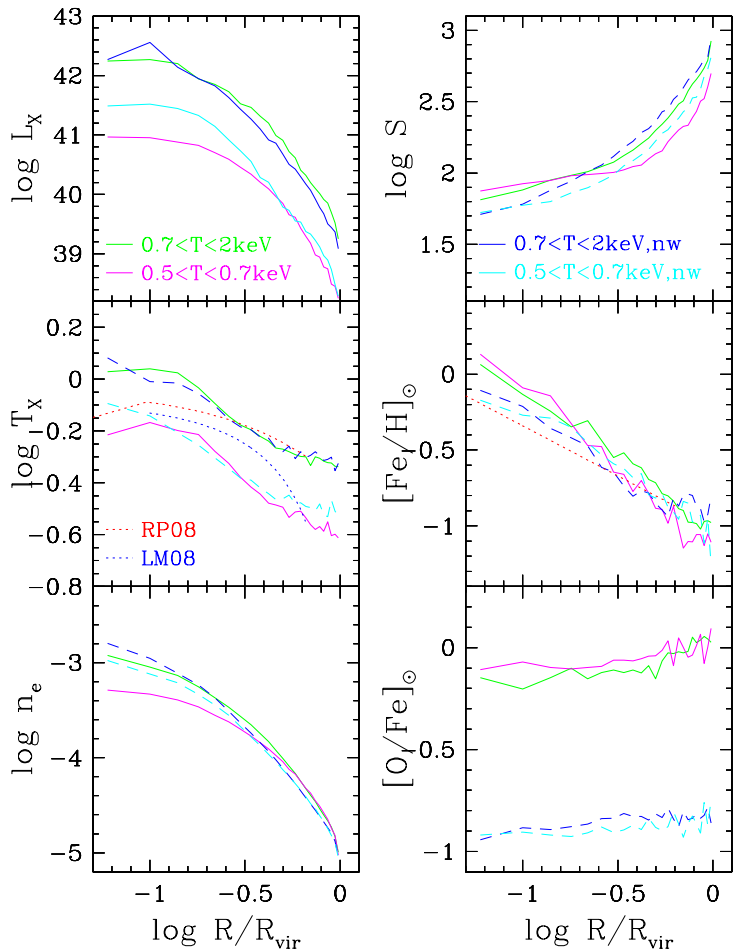


Figure 6. Radial profiles of physical quantities in our momentum-driven wind simulation. Profiles shown are medians over all galaxy groups within two bins: $0.7 < T_X < 2$ keV (green) and $0.5 < T_X < 0.7$ keV (magenta); each bin contains ≈ 40 groups. Blue and cyan curves show median profiles of groups in those two temperature ranges from the no-wind simulation. Note that there is significant scatter in individual profile shapes, which is not shown. Dotted lines in T_X and $[\text{Fe}/\text{H}]$ panels shows observations; red are from Rasmussen & Ponman (2007), blue are from Leccardi & Molendi (2008). *Top:* X-ray luminosity (erg/s); *Second:* X-ray luminosity-weighted temperature (keV); *Third:* Free electron density (cm^{-3}); *Fourth:* Entropy (keV cm^2); *Fifth:* Luminosity-weighted iron abundance; *Bottom:* Oxygen to iron ratio.

counting of various systematic effects such as background contamination and biases from low surface brightness regions (Leccardi & Molendi 2007), but other groups' results are similar (de Grandi & Molendi 2002; Vikhlinin et al. 2005). Although the observed clusters are not as directly comparable to our simulated groups, they may be more accurate particularly in the outer regions, and since the profile shapes seem to be mostly independent of system size, they may still be relevant.

The simulated T_X profiles appear mildly steeper than observations at $r > 0.1R_{\text{vir}}$, as has historically been seen in such comparisons, (e.g. Markevitch et al. 1998). There may be some additional source of thermalization such as cosmic rays or conduction that serves to flatten the real temper-

ature profiles. So long as such a process only moves heat and not mass or metals around, then the remaining physical profiles should not be significantly affected by fixing this discrepancy. At smaller radii, we do not have the resolution to reliably probe the temperature profile too far in, but the observed profiles show a drop towards the center that is similar to but steeper than seen in simulations (at least for the larger groups). This may result from an excess of star formation in the simulated central group galaxies are over-heating the core. Overall, the agreement with temperature profiles are reasonably good but not perfect.

The observed iron abundance profiles are in reasonable agreement with observations. There is a hint that the simulated abundance profiles are steeper than observed, but in this case the uncertainties are large enough (particularly in the outer regions) that the differences are probably not significant. Our simulations may also not be resolving the outer iron abundance profile ($r \gtrsim 0.3R_{\text{vir}}$) at our numerical resolution (Tornatore et al. 2007). Outflows do not greatly impact the iron abundance profile, because the stellar distribution is not altered significantly by outflows even though they suppress star formation overall.

The hot gas density profile shows a clear impact from outflows at $T_X \lesssim 1$ keV. The n_e profile is significantly shallower in the central region for lower-mass groups in the outflow run. In contrast, the no-wind run shows little difference between the two mass bins, although the increased efficiency of low-entropy gas removal does cause the smaller systems to have slightly flatter inner profiles. This demonstrates that outflows are important for further breaking self-similarity in the core regions of poor groups as observed.

The entropy profiles are also affected by outflows. The profiles from the wind run are significantly shallower than those from the no-wind run. Furthermore, less massive groups show a shallower profile relative to more massive systems. The outer profiles generally approach a slope of 1.1 expected for shock heating, but smaller systems do so further out. PSF03 measured entropy profiles that look qualitatively similar, showing a slope shallower than 1.1 out to R_{500} , particularly for smaller systems.

Finally, the alpha enrichment profiles (here traced by [O/Fe]) show a clear difference in amplitude between no-wind and wind runs. This reflects the overall alpha enrichment difference seen in Figure 1. More subtly, the no-wind runs show almost no gradient in [O/Fe], while a mild gradient is seen in the wind run. Still, the gradient is generally not as strong as observed in groups. Rasmussen & Ponman (2007) found that silicon to iron increased by a factor of 2.5 from $0.1 - 1R_{500}$, whereas our predicted [O/Fe] only increases by 40% over a comparable range. This may be owing to excess central star formation in our simulated groups that raises the central oxygen abundance.

Overall, the X-ray profiles give a more detailed view of the physics affected by outflow energy input as a function of mass. Winds are seen to clearly affect the gas density profile (and hence the entropy profile), as well as the alpha element abundance profile. Comparisons with observations yield general agreement, though in detail significant differences remain. Hence these simulations do not completely explain all observed group properties, even though global X-ray luminosity-weighted properties are fairly well reproduced. As detailed X-ray profile observations of groups im-

prove, matching them should yield insights into other feedback or heat conduction processes operating within intragroup gas.

6 CONCLUSIONS

Using Λ CDM cosmological hydrodynamic simulations of galaxy formation including galactic outflows and a sophisticated chemical enrichment model, we have studied the distribution and evolution of metals and entropy in galaxy groups. The one-line summary is that our simulation with outflow scalings as expected for momentum-driven winds is broadly successful at reproducing both the enrichment and entropy level seen in X-ray emitting intragroup gas. In more detail, we find:

- Our model with outflows reproduces the observed iron abundance of intragroup gas, while maintaining a stellar baryon fraction in broad agreement with observed values. The iron abundance is somewhat higher than seen for rich clusters, but then drops for $T_X \lesssim 0.5$ keV systems.
- Predictions for [O/Fe] in X-ray emitting gas are strongly affected by outflows. Our momentum-driven wind model is successful at reproducing the [O/Fe] ratio observed for clusters. Without outflows the oxygen abundance is too low, although it may be that our SPH-based code is underestimating the effectiveness of gas (and metal) stripping. Measurements of [O/Fe] in the poor group regime should provide stringent constraints on outflow models.
- The mass-weighted and X-ray luminosity weighted [O/Fe] ratio within groups can be significantly different. This suggests that [O/Fe] in X-ray luminous gas is a poor indicator of the relative contributions of Type II and Type Ia supernovae within the group as a whole, and is instead governed primarily by the effectiveness of distribution mechanisms for oxygen and iron.
- Iron abundance evolution predicted for groups is in general agreement with that seen for rich clusters, i.e. roughly a factor of two increase from $z = 1 \rightarrow 0$. Our simulations predict that [O/Fe] decreases by $\sim 30\%$ over the same time span, though halting late-time star formation in central group galaxies may increase such evolution.
- The total baryon fraction in groups is predicted to be somewhat below the cosmic mean baryon fraction, owing to pressure support from hot gas. In our outflow model this deficit increases in lower mass systems owing to ejection of halo baryons, while without winds the baryon fraction exceeds the cosmic value in the poorest groups.
- The core ($0.1R_{\text{vir}}$) entropy level of poor groups is found to scale as $S_{0.1} \propto T_X^{0.6}$, in agreement with observations by Ponman, Sanderson, & Finoguenov (2003). Much of the entropy increase over self-similar scaling owes to radiative cooling alone, but outflows add significant entropy to systems below 1 keV.
- Entropy at R_{500} is elevated from self-similar scalings, in broad agreement with observations. However, the scaling with temperature within the poor group regime is close to self-similarity. Outflows have essentially no impact here, as the elevation of S_{500} owes purely to the removal of low-entropy gas via radiative cooling.
- The amount of energy per baryon added to hot intragroup gas drops with increasing system size, and exceeds

the thermal energy below 0.5 keV. As a result, the $L_X - T_X$ relation shows a clear break below 1 keV. Both the $L_X - T_X$ and $\sigma - T_X$ relations predicted from our momentum-driven wind run are in good agreement with observations.

- Profiles of T_X and $[\text{Fe}/\text{H}]$ are qualitatively similar to observed, though model profiles appear to be somewhat steeper than data. The alpha enhancement profile is also quite shallow. Possible causes include missing heat transport mechanisms and an excess of late-time star formation in the central galaxy.

- Outflow energy injection makes the density and entropy profiles shallower at $T_X \lesssim 1$ keV, particularly in the inner regions.

The simultaneous success of enrichment and entropy injection from our momentum-driven wind outflows is a significant achievement, especially considering that this outflow model was not tuned in any way to match observations of intragroup gas. While the iron abundance is not very sensitive to outflows, the oxygen to iron ratio provides a key diagnostic that is well reproduced by our outflow model. Most of the entropy increase actually owes to radiative cooling, but outflows serve both to enrich intragroup gas as well as lower the stellar content to bring it more into line with observations.

The implication of our models is that pre-heating in intragroup gas arises from radiative cooling together with the same galactic outflows required to, for instance, enrich the IGM at high redshifts or establish the mass-metallicity relationship of galaxies. Hence the source of pre-heating may not be a mysterious widespread energy injection at high redshifts, nor be related to AGN feedback at lower redshifts. While something like AGN feedback is still required to truncate star formation in the central galaxy, our results suggest that it need not be a significant contributor to the overall entropy budget of intragroup gas. This eases the tension between a feedback process that must operate on dense central gas to prevent cooling flows (and therefore requires large amounts of energy to significantly increase entropy, since $S \propto n^{-2/3}$), and the need to raise the entropy of the more diffuse intragroup medium.

Nevertheless, there are certainly still significant problems with our simulations as-is, most notably the excess of late-time star formation in the central galaxy that may be responsible for poor fits to observed X-ray profiles. There is also the issue of the observed scatter in the X-ray scaling relations, which points to some more stochastic form of energy injection. Finally, it appears that large galaxy clusters also have elevated entropies all the way out to their outer regions (Dunn & Fabian 2008). Since wind energy cannot be responsible because it is less important in higher mass systems, this suggests that AGN energy, perhaps transported via buoyant bubbles, are needed to explain the thermodynamics of clusters.

A complete understanding of hot diffuse gas in groups and clusters will only come when a model addresses all three ICM issues simultaneously, namely the cooling flow, entropy, and metallicity problems. Our current simulations explicitly do not do so, focusing on two of the three problems solely in the poor group regime. Hence although our simulations suggest that entropy injection is tied mostly to metal enrichment and not cooling flow prevention, we forward this

interpretation only a suggestion and not a definitive statement. This must still be tested using simulations that self-consistently incorporate some mechanism to quench star formation in massive galaxies in accord with cluster galaxy data. We are actively pursuing such investigations.

There are two immediate paths for future investigations. The first is to incorporate some physical or heuristic model of star formation truncation in massive galaxies, in order to understand its impact on energy and metal input into intragroup gas. The second is to study how the enrichment and entropy of intragroup gas grow with redshift within a hierarchical framework, in order to better understand its physical origin. We also plan to continue developing tools to provide closer comparisons with observations, such as the ability to produce simulated X-ray maps that can be analyzed alongside data. Finally, we are planning to run significantly larger simulations with up to 2×512^3 particles in the near future, which will allow us to have greater dynamic range, study larger clusters, and properly assess resolution effects. While our initial efforts towards understanding intragroup gas chemo- and thermodynamics from outflows seem promising, there is much work to be done to fully understand the interplay between galaxy formation processes and the X-ray emitting plasma in the largest bound structures in the Universe.

ACKNOWLEDGEMENTS

The simulations used here were run at the National Center for Supercomputing Applications, as well as the University of Arizona's campus supercomputers. We thank Mark Dickinson, Mark Fardal, Neal Katz, Dusan Keres, Trevor Ponman, David Weinberg, and the referee for helpful suggestions. Support for this work was provided by NASA through grant number HST-AR-10946 from the SPACE TELESCOPE SCIENCE INSTITUTE, which is operated by AURA, Inc. under NASA contract NAS5-26555, as well as through grant ATP grant NNG06GH98G. Support for this work, part of the Spitzer Space Telescope Theoretical Research Program, was also provided by NASA through a contract issued by the Jet Propulsion Laboratory, California Institute of Technology under a contract with NASA. Support was also provided by the National Science Foundation through grant number DMS-0619881.

REFERENCES

- Agertz, O. et al. 2007, MNRAS, 380, 963
- Aguirre, A., Hernquist, L., Schaye, J., Katz, N., Weinberg, D. H., Gardner, J. 2001, ApJ, 561, 521
- Anders, E. & Grevesse, N. 1989, GeCoA, 53, 197
- Babul, A., Balogh, M. L., Lewis, G. F., Poole, G. B. 2002, MNRAS, 330, 329
- Baldry, I. K., Glazebrook, K., Driver, S. P. 2008, MNRAS, in press, arXiv:0804.2892
- Balestra, I., Tozzi, P., Ettori, S., Rosati, P., Borgani, S., Mainieri, V., Norman, C., Viola, M. 2007, A&A, 462, 429
- Balogh, M. L., Babul, A., Patton, D. R. 1999, MNRAS, 307, 463

- Balogh, M. L., Babul, A., Voit, G. M., McCarthy, I. G., Jones, L. R., Lewis, G. F., Ebeling, H. 2006, MNRAS, 366, 624
- Balogh, M. L. et al. 2007, MNRAS, 374, 1169
- Bell, E. F., McIntosh, D. H., Katz, N., Weinberg, M. D. 2003, ApJ, 585, L117
- Berlind, A. A., Weinberg, D. H., Benson, A. J., Baugh, C. M., Cole, S., Davé, R., Frenk, C. S., Jenkins, A., Katz, N., Lacey, C. G. 2003, ApJ, 593, 1
- Borgani, S., Finoguenov, A., Kay, S. T., Ponman, T. J., Springel, V., Tozzi, P., Voit, G. M. 2005, MNRAS, 361, 233
- Borgani, S., Fabjan, D., Tornatore, L., Schindler, S., Dolag, K., Diaferio, A. 2008, Space Sci. Rev., 134, 379
- Bouwens, R. J., Illingworth, G. D., Franx, M., Ford, H. 2007, ApJ, 670, 928
- Bower, R. G. 1997, MNRAS, 288, 355
- Bower, R. G., Benson, A. J., Lacey, C. G., Baugh, C. M., Cole, S., & Frenk, C. S. 2001, MNRAS, 325, 497
- Bower, R. G., Benson, A. J., Malbon, R., Helly, J. C., Frenk, C. S., Baugh, C. M., Cole, S., & Lacey, C. G. 2006, MNRAS, 370, 645
- Bruzual, G. & Charlot, S. 2003, MNRAS, 344, 1000
- Bryan, G. L. 2000, ApJ, 544, L1
- Burns, J. O., Hallman, E. J., Gantner, B., Motl, P. M., Norman, M. L. 2008, ApJ, 675, 1125
- Calura, F. & Matteucci, F. 2004, MNRAS, 351, 384
- Cen, R. & Ostriker, J. P. 1999, ApJ, 514, 1
- Cen, R. & Ostriker, J. P. 1999, ApJ, 519, L109
- Cen, R., Tripp, T. M., Ostriker, J. P., Jenkins, E. B. 2001, ApJ, 559, L5
- Chen, X., Weinberg, D. H., Katz, N., & Davé, R. 2003, ApJ, 594, 42
- Dalla Vecchia, C. & Schaye, J. 2008, MNRAS, accepted, arXiv:0801.2770
- Davé, R., Cen, R., Ostriker, J. P., Bryan, G. L., Hernquist, L., Katz, N., Weinberg, D. H., Norman, M. L., & O'Shea, B. 2001, ApJ, 552, 473
- Davé, R., Katz, N., Weinberg, D. H. 2002, ApJ, 579, 23
- Davé, R., Finlator, K., & Oppenheimer, B. D. 2006, MNRAS, 370, 273
- Davé, R. 2008, MNRAS, in press, arXiv:0710.0381
- Davis, D. S., Mulchaey, J. S., Mushotzky, R. F. 1999, ApJ, 511, 34
- De Grandi, S. & Molendi, S. 2002, ApJ, 567, 163
- De Grandi, S., Ettori, S., Longhetti, M., Molendi, S. 2004, A&A, 419, 7
- Dekel, A. & Birnboim, Y. 2008, MNRAS, 383, 119
- Dunn, R. J. H. & Fabian, A. C. 2008, MNRAS, 385, 757
- Eisenstein, D. J. & Hu, W. 1999, ApJ, 511, 5
- Eke, V. R., Navarro, J. F., Frenk, C. S. 1998, ApJ, 503, 569
- Ellison, S. L., Kewley, L. J., Mallén-Ornelas, G. 2005, MNRAS, 357, 354
- Erb, D. K., Shapley, A. E., Pettini, M., Steidel, C. C., Reddy, N. A., & Adelberger, K. L. 2006, ApJ, accepted, astro-ph/0602473
- Erb, D. K. 2008, ApJ, 674, 151
- Evrard, A. E. et al. 2008, ApJ, 672, 122
- Fabian, A. C., Nulsen, P. E. J., Canizares, C. R. 1984, Nature, 310, 733
- Fabjan, D., Tornatore, L., Borgani, S., Saro, A., Dolag, K. 2008, MNRAS, in press, arXiv:0802.2224
- Ferland, G., Korista, K. T., Verner, D. A., Ferguson, J. W., Kingdon, J. B., Verner, E. M. 1998, PASP, 110, 761
- Ferrara, A., Scannapieco, E., Bergeron, J. 2005, ApJ, 634, L37 [FSB05]
- Finlator, K., Davé, R., Papovich, C., & Hernquist, L. 2006, ApJ, 639, 672
- Finlator, K. & Davé, R. 2008, MNRAS, in press
- Finoguenov, A., Burkert, A., Boehringer, H. 2003, ApJ, 594, 136
- Gonzalez, A. H., Zaritsky, D., Zabludoff, A. I. 2007, ApJ, 666, 147
- Guo, F. & Oh, S. P. 2008, MNRAS, 384, 251
- Haardt, F. & Madau, P. 2001, in proc. XXXVIth Rencontres de Moriond, eds. D.M. Neumann & J.T.T. Van.
- Helsdon, S. F. & Ponman, T. J. 2000, MNRAS, 315, 356
- Jubelgas, M., Springel, V., Dolag, K. 2004, MNRAS, 351, 423
- Kennicutt, R. C. 1998, ApJ, 498, 541
- Kaiser, N. 1986, MNRAS, 222, 323
- Kaiser, N. 1991, ApJ, 383, 104
- Kay, S. 2004, MNRAS, 347, L13
- Kapferer, W., Kronberger, T., Weratschnig, J., Schindler, S., Domainko, W., van Kampen, E., Kimeswenger, S., Mair, M., Ruffert, M. 2007, A&A, 466, 813
- Keres, D., Katz, N., Weinberg, D. H., & Davé, R. 2005, MNRAS, in press
- Kim, W.-T. & Narayan, R. 2003, ApJ, 596, 889
- Kim, W.-T. & Narayan, R. 2003, ApJL, 596, L139
- Komatsu, E. et al. 2008, ApJS, submitted, arXiv:0803.0547
- Leccardi, A. & Molendi, S. 2007, A&A, 471, 21
- Leccardi, A. & Molendi, S. 2008, A&A, in press, arXiv:0804.1909
- Lin, Y.-T. & Mohr, J. J. 2004, ApJ, 617, 879
- Loken, C., Norman, M. L., Nelson, E., Burns, J., Bryan, G. L., Motl, P. 2002, ApJ, 579, 571
- Madau, P., Ferguson, H. C., Dickinson, M. E., Giavalisco, M., Steidel, C. C., Fruchter, A. 1996, MNRAS, 283, 1388
- Mannucci, F., Della Valle, M., Panagia, N., Cappellaro, E., Cresci, G., Maiolino, R., Petrosian, A., Turatto, M. 2005, A&A, 433, 807
- Markevitch, M., Forman, W. R., Sarazin, C. L., Vikhlinin, A. 1998, ApJ, 503, 77
- Martin, C. L. 2005, ApJ, 621, 227
- Maughan, B. J., Jones, C., Forman, W., Van Speybroeck, L. 2008, ApJS, 174, 117
- McCarthy, I. G., Babul, A., Balogh, M. L. 2002, ApJ, 573, 515
- McCarthy, I. G., Babul, A., Bower, R. G., Balogh, M. L. 2008, MNRAS, in press
- McNamara, B. R. & Nulsen, P. E. J. 2007, ARA&A, 45, 117
- Mo, H. J., Mao, S., & White, S. D. M. 1998, MNRAS, 295, 319
- Muanwong, O., Thomas, P. A., Kay, S. T., Pearce, F. R. 2002, MNRAS, 336, 527
- Muanwong, O., Kay, S. T., Thomas, P. A. 2006, ApJ, 649, 640
- Mulchaey, J. S. 2000, ARA&A, 38, 289
- Murray, N., Quatert, E., & Thompson, T. A. 2005, ApJ, 618, 569
- Navarro, J. F., Frenk, C. S., White, S. D. M. 1995, MNRAS, 275, 720

- Oppenheimer, B. D. & Davé, R. 2006, MNRAS, 373, 1265
- Oppenheimer, B. D. & Davé, R. 2008, MNRAS, in press
- Osmond, J. P. F. & Ponman, T. J. 2004, MNRAS, 350, 1511
- Pagel, B. E. J. 2002, in “Chemical Enrichment of Intracluster and Intergalactic Medium”, ASP conf. proc. v.253, eds. R. Fusco-Femiano and F. Matteucci, p.489
- Pei, Y. C., Fall, S. M., Hauser, M. G. 1999, ApJ, 522, 604
- C. Peroux, J. D. Meiring, V. P. Kulkarni, R. Ferlet, P. Khare, J. T. Lauroesch, G. Vladilo, D. G. York 2006, MNRAS, accepted, astro-ph/0607561
- Peterson, J. R., Kahn, S. M., Paerels, F. B. S., Kaastra, J. S., Tamura, T., Bleeker, J. A. M., Ferrigno, C., Jernigan, J. G. 2003, ApJ, 590, 207
- Peterson, J. R. & Fabian, A. C. 2006, PhysRep, 427, 1
- Pettini, M. 1999, in proc. ESO Workshop: ‘Chemical Evolution from Zero to High Redshift’, eds. J. Walsh & M. Rosa, astro-ph/9902173
- Pettini, M. 2004, in proc. “Cosmochemistry. The melting pot of the elements”, eds. C. Esteban, R. J. Garcí López, A. Herrero, F. Sánchez, Cambridge, UK: Cambridge University Press, p.257
- Pipino, A., Matteucci, F., Borgani, S., & Biviano, A. 2002, NewA, 7, 227
- Ponman, T. J., Cannon, D. B., & Navarro, J. F. 1999, Nature, 397, 135
- Ponman, T. J., Sanderson, A. J. R., Finoguenov, A. 2003, MNRAS, 343, 331
- Portinari, L., Moretti, A., Chiosi, C., Sommer-Larsen, J. 2004, ApJ, 604, 579
- Rasmussen, J. & Ponman, T. J. 2007, MNRAS, 380, 1554
- Renzini, A. 1997, ApJ, 488, 35
- Renzini, A. 2001, in proc. “Large Scale Structure in the X-ray Universe”, eds. Plionis, M. & Georgantopoulos, I., Atlantisciences, Paris, France, p.103
- Rosati, P. et al. 2004, AJ, 127, 230
- Rupke, D. S., Veilleux, S., & Sanders, D. B. 2005, ApJS, 160, 115
- Ryan-Weber, E. V., Pettini, M., & Madau, P. 2006, MNRAS, accepted, astro-ph/0607029
- Savaglio, S. et al. 2005, ApJ, 635, 260
- Scannapieco, E. & Bildsten, L. 2005 ApJ, 629, L85
- Sembach, K. R. et al. 2005, BAAS, 23.09, v. 37, p. 1197
- Shapley, A. E., Erb, D. K., Pettini, M., Steidel, C. C., Adelberger, K. L. 2004, ApJ, 612, 108
- Shapley, A. E., Steidel, C. C., Erb, D. K., Reddy, N. A., Adelberger, K. L., Pettini, M., Barmby, P., Huang, J. 2005, ApJ, 626, 698
- Smith, R. K., Brickhouse, N. S., Liedahl, D. A., Raymond, J. C. 2001, ApJL, 556, L91
- Sivanandam, S. et al., in preparation
- Sijacki, D., Pfrommer, C., Springel, V., Ensslin, T. A. 2008, MNRAS, submitted, arXiv:0801.3285
- D. N. Spergel *et al.*, ApJ, submitted, astro-ph/0603449
- Springel, V. & Hernquist, L. 2002, MNRAS, 333, 649
- Springel, V. & Hernquist, L. 2003, MNRAS, 339, 289
- Springel, V. & Hernquist, L. 2003, MNRAS, 339, 312
- Springel, V. 2005, MNRAS, 364, 1105
- Steidel, C. C., Shapley, A. E., Pettini, M., Adelberger, K. L., Erb, D. K., Reddy, N. A., Hunt, M. P. 2004, ApJ, 604, 534
- Sutherland, R. S. & Dopita, M. A. 1993, ApJS, 88, 253
- Tornatore, L., Borgani, S., Dolag, K., Matteucci, F. 2007, MNRAS, 382, 1050
- Tremonti, C. A., Heckman, T. M., Kauffmann, G., et al. 2004, ApJ, 613, 898
- van Kampen, E. et al. 2007, NewAR, 51, 84
- Vikhlinin, A., Markevitch, M., Murray, S. S., Jones, C., Forman, W., Van Speybroeck, L. 2005, ApJ, 628, 655
- Voit, G. M. & Bryan, G. L. 2001, Nature, 414, 425
- Weiner, B. J. et al. 2008, ApJ, submitted, arXiv:0804.4686
- White, D. A., Jones, C., & Forman, W. 1997, MNRAS, 292, 419
- Xue, Y.-J. & Wu, X.-P. 2000, ApJ, 538, 65
- Zaritsky, D., Gonzalez, A. H., Zabludoff, A. I. 2004, ApJ, 613, L93